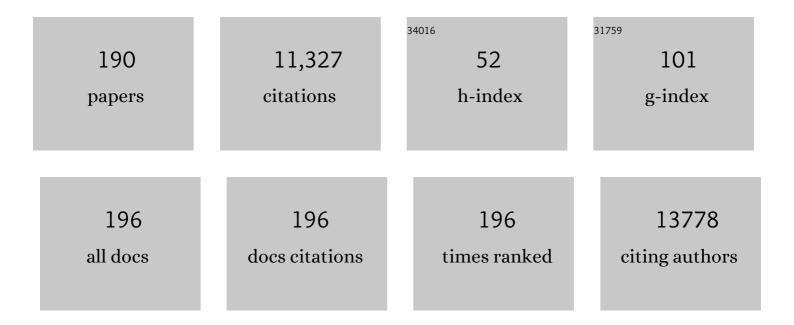
Libor Kovarik

List of Publications by Year in descending order

Source: https://exaly.com/author-pdf/3553596/publications.pdf Version: 2024-02-01



LIBOD KOUNDIK

#	Article	IF	CITATIONS
1	Activation of surface lattice oxygen in single-atom Pt/CeO ₂ for low-temperature CO oxidation. Science, 2017, 358, 1419-1423.	6.0	1,114
2	High capacity, reversible alloying reactions in SnSb/C nanocomposites for Na-ion battery applications. Chemical Communications, 2012, 48, 3321.	2.2	566
3	Highâ€Performance LiNi _{0.5} Mn _{1.5} O ₄ Spinel Controlled by Mn ³⁺ Concentration and Site Disorder. Advanced Materials, 2012, 24, 2109-2116.	11.1	434
4	Carbon-supported bimetallic Pd–Fe catalysts for vapor-phase hydrodeoxygenation of guaiacol. Journal of Catalysis, 2013, 306, 47-57.	3.1	384
5	CO ₂ Reduction on Supported Ru/Al ₂ O ₃ Catalysts: Cluster Size Dependence of Product Selectivity. ACS Catalysis, 2013, 3, 2449-2455.	5.5	376
6	Heterogeneous Catalysis on Atomically Dispersed Supported Metals: CO ₂ Reduction on Multifunctional Pd Catalysts. ACS Catalysis, 2013, 3, 2094-2100.	5.5	310
7	Tuning Pt-CeO2 interactions by high-temperature vapor-phase synthesis for improved reducibility of lattice oxygen. Nature Communications, 2019, 10, 1358.	5.8	302
8	Toward Rational Design of Cu/SSZ-13 Selective Catalytic Reduction Catalysts: Implications from Atomic-Level Understanding of Hydrothermal Stability. ACS Catalysis, 2017, 7, 8214-8227.	5.5	278
9	Thermally Stable and Regenerable Platinum–Tin Clusters for Propane Dehydrogenation Prepared by Atom Trapping on Ceria. Angewandte Chemie - International Edition, 2017, 56, 8986-8991.	7.2	262
10	In Situ TEM Investigation of Congruent Phase Transition and Structural Evolution of Nanostructured Silicon/Carbon Anode for Lithium Ion Batteries. Nano Letters, 2012, 12, 1624-1632.	4.5	256
11	Stabilizing High Metal Loadings of Thermally Stable Platinum Single Atoms on an Industrial Catalyst Support. ACS Catalysis, 2019, 9, 3978-3990.	5.5	233
12	Identification of the active complex for CO oxidation over single-atom Ir-on-MgAl2O4 catalysts. Nature Catalysis, 2019, 2, 149-156.	16.1	222
13	Low-Temperature Pd/Zeolite Passive NO _{<i>x</i>} Adsorbers: Structure, Performance, and Adsorption Chemistry. Journal of Physical Chemistry C, 2017, 121, 15793-15803.	1.5	178
14	Metallurgical Characterization of a New Nickel-Titanium Wire for Rotary Endodontic Instruments. Journal of Endodontics, 2009, 35, 1589-1593.	1.4	173
15	Enhanced Li+ ion transport in LiNi0.5Mn1.5O4 through control of site disorder. Physical Chemistry Chemical Physics, 2012, 14, 13515.	1.3	167
16	Stable platinum nanoparticles on specific MgAl2O4 spinel facets at high temperatures in oxidizing atmospheres. Nature Communications, 2013, 4, 2481.	5.8	166
17	Reductive Sequestration of Pertechnetate (⁹⁹ TcO ₄ [–]) by Nano Zerovalent Iron (nZVI) Transformed by Abiotic Sulfide. Environmental Science & Technology, 2013, 47, 5302-5310.	4.6	162
18	Revealing the Atomic Restructuring of Pt–Co Nanoparticles. Nano Letters, 2014, 14, 3203-3207.	4.5	162

#	Article	IF	CITATIONS
19	Determining the location and nearest neighbours of aluminium in zeolites with atom probe tomography. Nature Communications, 2015, 6, 7589.	5.8	139
20	Colloidal nanoparticle size control: experimental and kinetic modeling investigation of the ligand–metal binding role in controlling the nucleation and growth kinetics. Nanoscale, 2017, 9, 13772-13785.	2.8	137
21	Towards data-driven next-generation transmission electron microscopy. Nature Materials, 2021, 20, 274-279.	13.3	130
22	Achieving Atomic Dispersion of Highly Loaded Transition Metals in Smallâ€Pore Zeolite SSZâ€13: Highâ€Capacity and Highâ€Efficiency Lowâ€Temperature CO and Passive NO _{<i>x</i>} Adsorbers. Angewandte Chemie - International Edition, 2018, 57, 16672-16677.	7.2	129
23	Effect of preparation methods on the performance of Co/Al ₂ O ₃ catalysts for dry reforming of methane. Green Chemistry, 2014, 16, 885-896.	4.6	122
24	Structure Sensitivity of Acetylene Semi-Hydrogenation on Pt Single Atoms and Subnanometer Clusters. ACS Catalysis, 2019, 9, 11030-11041.	5.5	111
25	Effect of metal–support interactions in Ni/Al2O3 catalysts with low metal loading for methane dry reforming. Applied Catalysis A: General, 2015, 494, 57-67.	2.2	106
26	Highly active and stable MgAl2O4-supported Rh and Ir catalysts for methane steam reforming: A combined experimental and theoretical study. Journal of Catalysis, 2014, 316, 11-23.	3.1	104
27	Reduction and immobilization of hexavalent chromium by microbially reduced Fe-bearing clay minerals. Geochimica Et Cosmochimica Acta, 2014, 133, 186-203.	1.6	103
28	Molecular Level Understanding of How Oxygen and Carbon Monoxide Improve NO _{<i>x</i>} Storage in Palladium/SSZ-13 Passive NO _{<i>x</i>} Adsorbers: The Role of NO ⁺ and Pd(II)(CO)(NO) Species. Journal of Physical Chemistry C, 2018, 122, 10820-10827.	1.5	101
29	Effect of Oxygen Defects on the Catalytic Performance of VO _{<i>x</i>} /CeO ₂ Catalysts for Oxidative Dehydrogenation of Methanol. ACS Catalysis, 2015, 5, 3006-3012.	5.5	96
30	Transformation of Active Sites in Fe/SSZ-13 SCR Catalysts during Hydrothermal Aging: A Spectroscopic, Microscopic, and Kinetics Study. ACS Catalysis, 2017, 7, 2458-2470.	5.5	89
31	Copper-zirconia interfaces in UiO-66 enable selective catalytic hydrogenation of CO2 to methanol. Nature Communications, 2020, 11, 5849.	5.8	86
32	Reduction of U(VI) Incorporated in the Structure of Hematite. Environmental Science & Technology, 2012, 46, 9428-9436.	4.6	82
33	Synthesis and Hydrodeoxygenation Properties of Ruthenium Phosphide Catalysts. ACS Catalysis, 2011, 1, 917-922.	5.5	81
34	Tomography and High-Resolution Electron Microscopy Study of Surfaces and Porosity in a Plate-like γ-Al ₂ O ₃ . Journal of Physical Chemistry C, 2013, 117, 179-186.	1.5	81
35	Palladium/Beta zeolite passive NOx adsorbers (PNA): Clarification of PNA chemistry and the effects of CO and zeolite crystallite size on PNA performance. Applied Catalysis A: General, 2019, 569, 141-148.	2.2	81
36	XEDS STEM tomography for 3D chemical characterization of nanoscale particles. Ultramicroscopy, 2013, 131, 24-32.	0.8	78

#	Article	IF	CITATIONS
37	Structural analysis of a new precipitate phase in high-temperature TiNiPt shape memory alloys. Acta Materialia, 2010, 58, 4660-4673.	3.8	77
38	Size-Dependent Catalytic Performance of CuO on γ-Al ₂ O ₃ : NO Reduction versus NH ₃ Oxidation. ACS Catalysis, 2012, 2, 1432-1440.	5.5	75
39	Oxidative Remobilization of Technetium Sequestered by Sulfide-Transformed Nano Zerovalent Iron. Environmental Science & Technology, 2014, 48, 7409-7417.	4.6	73
40	Structure of δ-Alumina: Toward the Atomic Level Understanding of Transition Alumina Phases. Journal of Physical Chemistry C, 2014, 118, 18051-18058.	1.5	72
41	Airborne soil organic particles generated byÂprecipitation. Nature Geoscience, 2016, 9, 433-437.	5.4	71
42	Effect of the SiO2 support on the catalytic performance of Ag/ZrO2/SiO2 catalysts for the single-bed production of butadiene from ethanol. Applied Catalysis B: Environmental, 2018, 236, 576-587.	10.8	70
43	Environmental Transmission Electron Microscopy Study of the Origins of Anomalous Particle Size Distributions in Supported Metal Catalysts. ACS Catalysis, 2012, 2, 2349-2356.	5.5	68
44	Ni5Ca3 catalysts for CO2 reduction to methanol: Exploring the role of Ga surface oxidation/reduction on catalytic activity. Applied Catalysis B: Environmental, 2020, 267, 118369.	10.8	68
45	Stabilization of Super Electrophilic Pd ⁺² Cations in Small-Pore SSZ-13 Zeolite. Journal of Physical Chemistry C, 2020, 124, 309-321.	1.5	67
46	Effects of CeO2 support facets on VOx/CeO2 catalysts in oxidative dehydrogenation of methanol. Journal of Catalysis, 2014, 315, 15-24.	3.1	66
47	Synthesis of methanol and dimethyl ether from syngas over Pd/ZnO/Al2O3 catalysts. Catalysis Science and Technology, 2012, 2, 2116.	2.1	64
48	Synthesis of 1 nm Pd Nanoparticles in a Microfluidic Reactor: Insights from in Situ X-ray Absorption Fine Structure Spectroscopy and Small-Angle X-ray Scattering. Journal of Physical Chemistry C, 2015, 119, 13257-13267.	1.5	61
49	The role of nanoparticle size and ligand coverage in size focusing of colloidal metal nanoparticles. Nanoscale Advances, 2019, 1, 4052-4066.	2.2	61
50	High-resolution characterization of the precipitation behavior of an Al–Zn–Mg–Cu alloy. Philosophical Magazine Letters, 2012, 92, 166-178.	0.5	59
51	Dendrimerâ€Encapsulated Ruthenium Oxide Nanoparticles as Catalysts in Lithiumâ€Oxygen Batteries. Advanced Functional Materials, 2014, 24, 7510-7519.	7.8	59
52	Sorption-enhanced synthetic natural gas (SNG) production from syngas: A novel process combining CO methanation, water-gas shift, and CO2 capture. Applied Catalysis B: Environmental, 2014, 144, 223-232.	10.8	59
53	The superior hydrothermal stability of Pd/SSZ-39 in low temperature passive NOx adsorption (PNA) and methane combustion. Applied Catalysis B: Environmental, 2021, 280, 119449.	10.8	56
54	High temperature transition aluminas in δAl2O3/Î,-Al2O3 stability range: Review. Journal of Catalysis, 2021, 393, 357-368.	3.1	55

#	Article	IF	CITATIONS
55	Environment of Metal–O–Fe Bonds Enabling High Activity in CO ₂ Reduction on Single Metal Atoms and on Supported Nanoparticles. Journal of the American Chemical Society, 2021, 143, 5540-5549.	6.6	54
56	Disordered, Sub-Nanometer Ru Structures on CeO ₂ are Highly Efficient and Selective Catalysts in Polymer Upcycling by Hydrogenolysis. ACS Catalysis, 2022, 12, 4618-4627.	5.5	54
57	A General Mechanism for Stabilizing the Small Sizes of Precious Metal Nanoparticles on Oxide Supports. Chemistry of Materials, 2014, 26, 5475-5481.	3.2	53
58	Visualizing the iron atom exchange front in the Fe(II)-catalyzed recrystallization of goethite by atom probe tomography. Proceedings of the National Academy of Sciences of the United States of America, 2019, 116, 2866-2874.	3.3	52
59	Unraveling the Origin of Structural Disorder in High Temperature Transition Al ₂ O ₃ : Structure of Î,-Al ₂ O ₃ . Chemistry of Materials, 2015, 27, 7042-7049.	3.2	51
60	Inâ€Situ Dispersion of Palladium on TiO ₂ During Reverse Water–Gas Shift Reaction: Formation of Atomically Dispersed Palladium. Angewandte Chemie - International Edition, 2020, 59, 17657-17663.	7.2	51
61	Economizing on Precious Metals in Threeâ€Way Catalysts: Thermally Stable and Highly Active Singleâ€Atom Rhodium on Ceria for NO Abatement under Dry and Industrially Relevant Conditions**. Angewandte Chemie - International Edition, 2021, 60, 391-398.	7.2	51
62	Thermally Stable and Regenerable Platinum–Tin Clusters for Propane Dehydrogenation Prepared by Atom Trapping on Ceria. Angewandte Chemie, 2017, 129, 9114-9119.	1.6	49
63	A versatile approach for quantification of surface site fractions using reaction kinetics: The case of CO oxidation on supported Ir single atoms and nanoparticles. Journal of Catalysis, 2019, 378, 121-130.	3.1	49
64	In Situ X-ray Absorption Fine Structure Studies on the Effect of pH on Pt Electronic Density during Aqueous Phase Reforming of Glycerol. ACS Catalysis, 2012, 2, 2387-2394.	5.5	47
65	Reduced Magnetism in Core–Shell Magnetite@MOF Composites. Nano Letters, 2017, 17, 6968-6973.	4.5	47
66	Rupturing of Biological Spores As a Source of Secondary Particles in Amazonia. Environmental Science & Technology, 2016, 50, 12179-12186.	4.6	46
67	Steam reforming of hydrocarbons from biomass-derived syngas over MgAl2O4-supported transition metals and bimetallic IrNi catalysts. Applied Catalysis B: Environmental, 2016, 184, 142-152.	10.8	46
68	Microbe Encapsulation for Selective Rare-Earth Recovery from Electronic Waste Leachates. Environmental Science & Technology, 2019, 53, 13888-13897.	4.6	45
69	Conversion of Methane into Methanol and Ethanol over Nickel Oxide on Ceria–Zirconia Catalysts in a Single Reactor. Angewandte Chemie - International Edition, 2017, 56, 13876-13881.	7.2	44
70	Steam reforming of fast pyrolysis-derived aqueous phase oxygenates over Co, Ni, and Rh metals supported on MgAl2O4. Catalysis Today, 2016, 269, 166-174.	2.2	43
71	Grain boundary engineering to control the discontinuous precipitation in multicomponent U10Mo alloy. Acta Materialia, 2018, 151, 181-190.	3.8	43
72	Structural identification of ZnxZryOz catalysts for Cascade aldolization and self-deoxygenation reactions. Applied Catalysis B: Environmental, 2018, 234, 337-346.	10.8	43

#	Article	IF	CITATIONS
73	Cr(III) Adsorption by Cluster Formation on Boehmite Nanoplates in Highly Alkaline Solution. Environmental Science & Technology, 2019, 53, 11043-11055.	4.6	42
74	Formation of Oxygen Radical Sites on MoVNbTeOx by Cooperative Electron Redistribution. Journal of the American Chemical Society, 2017, 139, 12342-12345.	6.6	41
75	Effects of citrate on hexavalent chromium reduction by structural Fe(II) in nontronite. Journal of Hazardous Materials, 2018, 343, 245-254.	6.5	41
76	Ab initio analysis of Guinier–Preston–Bagaryatsky zone nucleation in Al–Cu–Mg alloys. Acta Materialia, 2012, 60, 3861-3872.	3.8	40
77	Comparative Investigation of Benzene Steam Reforming over Spinel Supported Rh and Ir Catalysts. ACS Catalysis, 2013, 3, 1133-1143.	5.5	39
78	Tc(VII) and Cr(VI) Interaction with Naturally Reduced Ferruginous Smectite from a Redox Transition Zone. Environmental Science & Technology, 2017, 51, 9042-9052.	4.6	38
79	Palladium/Zeolite Low Temperature Passive NOx Adsorbers (PNA): Structure-Adsorption Property Relationships for Hydrothermally Aged PNA Materials. Emission Control Science and Technology, 2020, 6, 126-138.	0.8	38
80	Reactivity of redox cycled Fe-bearing subsurface sediments towards hexavalent chromium reduction. Geochimica Et Cosmochimica Acta, 2019, 252, 88-106.	1.6	37
81	Onset of High Methane Combustion Rates over Supported Palladium Catalysts: From Isolated Pd Cations to PdO Nanoparticles. Jacs Au, 2021, 1, 396-408.	3.6	37
82	Competing Mechanisms in CO Hydrogenation over Co-MnO _{<i>x</i>} Catalysts. ACS Catalysis, 2019, 9, 5603-5612.	5.5	36
83	Single-Step Conversion of Ethanol to <i>n</i> Butene over Ag-ZrO ₂ /SiO ₂ Catalysts. ACS Catalysis, 2020, 10, 10602-10613.	5.5	34
84	Single-Facet Dominant Anatase TiO ₂ (101) and (001) Model Catalysts to Elucidate the Active Sites for Alkanol Dehydration. ACS Catalysis, 2020, 10, 4268-4279.	5.5	32
85	Automotive Brake Lining Characterization. , 0, , .		31
86	Inverse iron oxide/metal catalysts from galvanic replacement. Nature Communications, 2020, 11, 3269.	5.8	31
87	Irradiation effects and hydrogen behavior in H2+ and He+ implanted Î ³ -LiAlO2 single crystals. Journal of Nuclear Materials, 2017, 484, 374-381.	1.3	29
88	Quantification of Highâ€Temperature Transition Al ₂ O ₃ and Their Phase Transformations**. Angewandte Chemie - International Edition, 2020, 59, 21719-21727.	7.2	28
89	Effect of Water Vapor, Temperature, and Rapid Annealing on Formamidinium Lead Triiodide Perovskite Crystallization, ACS Energy Letters, 2016, 1, 155,161 Kinetics and mechanisms of cadmium carbonate heteroepitaxial growth at the calcite <mml:math< td=""><td>8.8</td><td>27</td></mml:math<>	8.8	27
00	xmlns:mml="http://www.w3.org/1998/Math/MathML" altimg="sil.gif" overflow="scroll"> <mml:mrow><mml:mo strateby="false", / / mml:me> / mml:me> 10 / mml:me> / mml:mspace width="0.12em" /> / mml:me>ver) Ti ETOo(</mml:mo </mml:mrow>		Ougetach 10

#	Article	IF	CITATIONS
91	Imaging the Optical Fields of Functionalized Silver Nanowires through Molecular TERS. Journal of Physical Chemistry Letters, 2018, 9, 7105-7109.	2.1	26
92	Precise Identification and Characterization of Catalytically Active Sites on the Surface of γâ€Alumina**. Angewandte Chemie - International Edition, 2021, 60, 17522-17530.	7.2	26
93	Steam Reforming of Acetic Acid over Co-Supported Catalysts: Coupling Ketonization for Greater Stability. ACS Sustainable Chemistry and Engineering, 2017, 5, 9136-9149.	3.2	25
94	Inorganic tin aluminophosphate nanocomposite for reductive separation of pertechnetate. Environmental Science: Nano, 2016, 3, 1003-1013.	2.2	24
95	Phase transformation of metastable discontinuous precipitation products to equilibrium phases in U10Mo alloys. Scripta Materialia, 2018, 156, 70-74.	2.6	24
96	Catalytic decomposition of methane into hydrogen and high-value carbons: combined experimental and DFT computational study. Catalysis Science and Technology, 2021, 11, 4911-4921.	2.1	24
97	Palladium/Ferrierite versus Palladium/SSZâ€1 3 Passive NOx Adsorbers: Adsorbateâ€Controlled Location of Atomically Dispersed Palladium(II) in Ferrierite Determines High Activity and Stability**. Angewandte Chemie - International Edition, 2022, 61, .	7.2	24
98	RedOx-controlled sorption of iodine anions by hydrotalcite composites. RSC Advances, 2016, 6, 76042-76055.	1.7	23
99	Conversion of syngas-derived C2+ mixed oxygenates to C3–C5 olefins over ZnxZryOz mixed oxide catalysts. Catalysis Science and Technology, 2016, 6, 2325-2336.	2.1	23
100	Electron transfer between sorbed Fe(II) and structural Fe(III) in smectites and its effect on nitrate-dependent iron oxidation by Pseudogulbenkiania sp. strain 2002. Geochimica Et Cosmochimica Acta, 2019, 265, 132-147.	1.6	23
101	Methane and Ethane Steam Reforming over MgAl2O4-Supported Rh and Ir Catalysts: Catalytic Implications for Natural Gas Reforming Application. Catalysts, 2019, 9, 801.	1.6	23
102	Probing Acid–Base Properties of Anatase TiO ₂ Nanoparticles with Dominant {001} and {101} Facets Using Methanol Chemisorption and Surface Reactions. Journal of Physical Chemistry C, 2021, 125, 3988-4000.	1.5	23
103	Structure sensitivity and its effect on methane turnover and carbon co-product selectivity in thermocatalytic decomposition of methane over supported Ni catalysts. Applied Catalysis A: General, 2021, 611, 117967.	2.2	23
104	Rate enhancement by Cu in Ni _x Cu _{1â^'x} /ZrO ₂ bimetallic catalysts for hydrodeoxygenation of stearic acid. Catalysis Science and Technology, 2019, 9, 2620-2629.	2.1	22
105	Influence of Ag metal dispersion on the thermal conversion of ethanol to butadiene over Ag-ZrO2/SiO2 catalysts. Journal of Catalysis, 2020, 386, 30-38.	3.1	22
106	Coupling of Methane to Ethane, Ethylene, and Aromatics over Nickel on Ceria–Zirconia at Low Temperatures. ChemCatChem, 2018, 10, 2700-2708.	1.8	21
107	Nanoscale observations of Fe(<scp>ii</scp>)-induced ferrihydrite transformation. Environmental Science: Nano, 2020, 7, 2953-2967.	2.2	21
108	Conversion of ethanol to 1,3–butadiene over Ag–ZrO2/SiO2 catalysts: The role of surface interfaces. Journal of Energy Chemistry, 2021, 54, 7-15.	7.1	21

#	Article	IF	CITATIONS
109	WO supported on \hat{I}^3 -Al2O3 with different morphologies as model catalysts for alkanol dehydration. Journal of Catalysis, 2018, 363, 1-8.	3.1	20
110	Revisiting the Growth Mechanism of Hierarchical Semiconductor Nanostructures: The Role of Secondary Nucleation in Branch Formation. Journal of Physical Chemistry Letters, 2019, 10, 6827-6834.	2.1	20
111	Catalytic activation of ethylene C–H bonds on uniform d ⁸ Ir(<scp>i</scp>) and Ni(<scp>ii</scp>) cations in zeolites: toward molecular level understanding of ethylene polymerization on heterogeneous catalysts. Catalysis Science and Technology, 2019, 9, 6570-6576.	2.1	20
112	Synthesis of nanometer-sized fayalite and magnesium-iron(II) mixture olivines. Journal of Colloid and Interface Science, 2018, 515, 129-138.	5.0	19
113	Surface engineering of earth-abundant Fe catalysts for selective hydrodeoxygenation of phenolics in liquid phase. Chemical Science, 2020, 11, 5874-5880.	3.7	19
114	Coupled Lattice Polarization and Ferromagnetism in Multiferroic NiTiO ₃ Thin Films. ACS Applied Materials & Interfaces, 2017, 9, 21879-21890.	4.0	18
115	Inâ€Situ Dispersion of Palladium on TiO ₂ During Reverse Water–Gas Shift Reaction: Formation of Atomically Dispersed Palladium. Angewandte Chemie, 2020, 132, 17810-17816.	1.6	18
116	Solvent manipulation of the pre-reduction metal–ligand complex and particle-ligand binding for controlled synthesis of Pd nanoparticles. Nanoscale, 2021, 13, 206-217.	2.8	18
117	Manganese-calcium intermixing facilitates heteroepitaxial growth at the <mmi:math xmlns:mml="http://www.w3.org/1998/Math/MathML" altimg="si3.gif" overflow="scroll"><mml:mfenced open="(" close=")"><mml:mrow><mml:mn>10</mml:mn><mml:mover accent="false"><mml:mn>1</mml:mn><td>1.4 ·ow><td>17 ll:mfenced><!--</td--></td></td></mml:mover </mml:mrow></mml:mfenced </mmi:math 	1.4 ·ow> <td>17 ll:mfenced><!--</td--></td>	17 ll:mfenced> </td
118	General Method for Determination of the Surface Composition in Bimetallic Nanoparticle Catalysts from the L Edge X-ray Absorption Near-Edge Spectra. ACS Catalysis, 2012, 2, 2433-2443.	5.5	16
119	Enhancing magnesite formation at low temperature and high CO2 pressure: The impact of seed crystals and minor components. Chemical Geology, 2015, 395, 119-125.	1.4	16
120	Temperature-Dependent Communication between Pt/Al ₂ O ₃ Catalysts and Anatase TiO ₂ Dilutant: the Effects of Metal Migration and Carbon Transfer on the Reverse Water–Gas Shift Reaction. ACS Catalysis, 2021, 11, 12058-12067.	5.5	16
121	Precise Identification and Characterization of Catalytically Active Sites on the Surface of γâ€Alumina**. Angewandte Chemie, 2021, 133, 17663-17671.	1.6	15
122	Optical Properties of Airborne Soil Organic Particles. ACS Earth and Space Chemistry, 2017, 1, 511-521.	1.2	14
123	Ligand-Mediated Nucleation and Growth of Palladium Metal Nanoparticles. Journal of Visualized Experiments, 2018, , .	0.2	14
124	Structural Intergrowth in δ-Al ₂ O ₃ . Journal of Physical Chemistry C, 2019, 123, 9454-9460.	1.5	14
125	Direct Catalytic Conversion of Ethanol to C ₅₊ Ketones: Role of Pd–Zn Alloy on Catalytic Activity and Stability. Angewandte Chemie - International Edition, 2020, 59, 14550-14557.	7.2	14
126	Calcareous organic matter coatings sequester siderophores in alkaline soils. Science of the Total Environment, 2020, 724, 138250.	3.9	14

#	Article	IF	CITATIONS
127	Magnesium behavior and structural defects in Mg+ ion implanted silicon carbide. Journal of Nuclear Materials, 2015, 458, 146-155.	1.3	13
128	Direct observation and assessment of phase states of ambient and lab-generated sub-micron particles upon humidification. RSC Advances, 2021, 11, 15264-15272.	1.7	13
129	Accessing crystal–crystal interaction forces with oriented nanocrystal atomic force microscopy probes. Nature Protocols, 2018, 13, 2005-2030.	5.5	12
130	Microbe-Encapsulated Silica Gel Biosorbents for Selective Extraction of Scandium from Coal Byproducts. Environmental Science & Technology, 2021, 55, 6320-6328.	4.6	12
131	Crystallographic and compositional analysis of impurity phase U2MoSi2C in UMo alloys. Journal of Nuclear Materials, 2019, 519, 287-291.	1.3	11
132	Kinetics and Mechanisms of ZnO to ZlFâ€8 Transformations in Supercritical CO 2 Revealed by Inâ€Situ Xâ€ray Diffraction. ChemSusChem, 2020, 13, 2602-2612.	3.6	11
133	Structure sensitivity of n-butane hydrogenolysis on supported Ir catalysts. Journal of Catalysis, 2021, 394, 376-386.	3.1	11
134	Understanding the Deactivation of Agâ^'ZrO ₂ /SiO ₂ Catalysts for the Singleâ€step Conversion of Ethanol to Butenes. ChemCatChem, 2021, 13, 999-1008.	1.8	11
135	Characterization of CoCu- and CoMn-Based Catalysts for the Fischer–Tropsch Reaction Toward Chain-Lengthened Oxygenates. Topics in Catalysis, 2018, 61, 1016-1023.	1.3	10
136	Silicate stabilisation of colloidal UO2 produced by uranium metal corrosion. Journal of Nuclear Materials, 2019, 526, 151751.	1.3	10
137	Facet-selective adsorption of Fe(<scp>ii</scp>) on hematite visualized by nanoscale secondary ion mass spectrometry. Environmental Science: Nano, 2019, 6, 2429-2440.	2.2	10
138	Economizing on Precious Metals in Threeâ€Way Catalysts: Thermally Stable and Highly Active Singleâ€Atom Rhodium on Ceria for NO Abatement under Dry and Industrially Relevant Conditions**. Angewandte Chemie, 2021, 133, 395-402.	1.6	10
139	Using Atom Dynamics to Map the Defect Structure Around an Impurity in Nano-Hematite. Journal of Physical Chemistry Letters, 2020, 11, 10396-10400.	2.1	9
140	Hierarchically structured catalysts for cascade and selective steam reforming/hydrodeoxygenation reactions. Chemical Communications, 2015, 51, 16617-16620.	2.2	8
141	Epitaxial single-crystal thin films of Mn Ti1â^'O2â^' grown on (rutile)TiO2 substrates with pulsed laser deposition: Experiment and theory. Surface Science, 2015, 632, 185-194.	0.8	8
142	Compressive STEM-EELS. Microscopy and Microanalysis, 2016, 22, 560-561.	0.2	8
143	Promoting the Cleavage of C–O Bonds at the Interface between a Metal Oxide Cluster and a Co(0001) Support. ACS Catalysis, 2020, 10, 14722-14731.	5.5	8
144	Elucidating the Active Site and the Role of Alkali Metals in Selective Hydrodeoxygenation of Phenols over Iron arbideâ€based Catalyst. ChemSusChem, 2021, 14, 4546-4555.	3.6	8

#	Article	IF	CITATIONS
145	Biomimetic CO oxidation below â^100 °C by a nitrate-containing metal-free microporous system. Nature Communications, 2021, 12, 6033.	5.8	8
146	Microstructure and Cs Behavior of Ba-Doped Aluminosilicate Pollucite Irradiated with F ⁺ Ions. Journal of Physical Chemistry C, 2014, 118, 18160-18169.	1.5	7
147	Stabilization and transformation of Pt nanocrystals supported on ZnAl2O4spinel. RSC Advances, 2017, 7, 3282-3286.	1.7	7
148	Grain Growth in Nanocrystalline Mg-Al Thin Films. Metallurgical and Materials Transactions A: Physical Metallurgy and Materials Science, 2017, 48, 6118-6125.	1.1	7
149	Heating-Induced Transformations of Atmospheric Particles: Environmental Transmission Electron Microscopy Study. Analytical Chemistry, 2018, 90, 9761-9768.	3.2	7
150	Singleâ€step Conversion of Methyl Ethyl Ketone to Olefins over Zn x Zr y O z Catalysts in Water. ChemCatChem, 2019, 11, 3393-3400.	1.8	7
151	Uncovering the active sites and demonstrating stable catalyst for the cost-effective conversion of ethanol to 1-butanol. Green Chemistry, 2021, 23, 8030-8039.	4.6	7
152	Structure and radiation damage behavior of epitaxial Cr Mo1â^' alloy thin films on MgO. Journal of Nuclear Materials, 2013, 437, 55-61.	1.3	6
153	Longâ€ŧerm accumulation, depth distribution, and speciation of silver nanoparticles in biosolidsâ€amended soils. Journal of Environmental Quality, 2020, 49, 1679-1689.	1.0	6
154	Redox-Based Electrochemical Affinity Sensor for Detection of Aqueous Pertechnetate Anion. ACS Sensors, 2020, 5, 674-685.	4.0	6
155	Microstructural evolution and precipitation in \hat{I}^3 -LiAlO2 during ion irradiation. Journal of Applied Physics, 2022, 131, .	1.1	6
156	Thin metal oxide films to modify a window layer in CdTe-based solar cells for improved performance. Applied Physics Letters, 2012, 100, 213908.	1.5	5
157	Surface enrichment of Pt in stable Pt-Ir nano-alloy particles on MgAl2O4 spinel in oxidizing atmosphere. Catalysis Communications, 2017, 93, 57-61.	1.6	5
158	Surface speciation and interactions between adsorbed chloride and water on cerium dioxide. Journal of Solid State Chemistry, 2018, 262, 16-25.	1.4	5
159	Environmental Transmission Electron Microscopy of Individual Atmospheric Particles from the North Atlantic. Microscopy and Microanalysis, 2018, 24, 396-397.	0.2	5
160	Characterization of slag and metal from uranium bomb reduction: Morphology, speciation, and the search for thorium. Materials Characterization, 2019, 158, 109948.	1.9	5
161	Effects of high-temperature CeO ₂ calcination on the activity of Pt/CeO ₂ catalysts for oxidation of unburned hydrocarbon fuels. Catalysis Science and Technology, 2022, 12, 2462-2470.	2.1	5
162	TEM Video Compressive Sensing. Microscopy and Microanalysis, 2015, 21, 1583-1584.	0.2	4

#	Article	IF	CITATIONS
163	CO oxidation on MgAl ₂ O ₄ supported Ir _{<i>n</i>} : activation of lattice oxygen in the subnanometer regime and emergence of nuclearity-activity volcano. Journal of Materials Chemistry A, 2022, 10, 4266-4278.	5.2	4
164	Deciphering the Distribution and Crystal-Chemical Environment of Arsenic, Lead, Silica, Phosphorus, Tin, and Zinc in a Porous Ferrihydrite Grain Using Transmission Electron Microscopy and Atom Probe Tomography. ACS Earth and Space Chemistry, 2022, 6, 558-570.	1.2	4
165	Compressive Sensing in Microscopy: a Tutorial. Microscopy and Microanalysis, 2016, 22, 2084-2085.	0.2	3
166	Controlling the structure and ferroic properties of strained epitaxial NiTiO3 thin films on sapphire by post-deposition annealing. Thin Solid Films, 2018, 662, 47-53.	0.8	3
167	Quantification of Highâ€Temperature Transition Al ₂ O ₃ and Their Phase Transformations**. Angewandte Chemie, 2020, 132, 21903-21911.	1.6	3
168	Implementing Sub-sampling Methods for Low-Dose (Scanning) Transmission Electron Microscopy (S/TEM). Microscopy and Microanalysis, 2017, 23, 82-83.	0.2	2
169	Implementing Sparse Sub-Sampling Methods for Low-Dose/High Speed STEM. Microscopy and Microanalysis, 2018, 24, 1952-1953.	0.2	2
170	Elemental iron: reduction of pertechnetate in the presence of silica and periodicity of precipitated nano-structures. Environmental Science: Nano, 2021, 8, 97-109.	2.2	2
171	Pd/FER vs Pd/SSZâ€13 Passive NOx Adsorbers: Adsorbateâ€controlled Location of Atomically Dispersed Pd(II) in FER Determines High Activity and Stability. Angewandte Chemie, 0, , .	1.6	2
172	GaN Nuclear Batteries: Radiation Modeling for the Accelerated Contact Exposure of Betavoltaics. MRS Advances, 2020, 5, 1483-1489.	0.5	2
173	Identification of Fragile Microscopic Structures during Mineral Transformations in Wet Supercritical CO2. Microscopy and Microanalysis, 2013, 19, 268-275.	0.2	1
174	Revealing the Working Active Sites of M1 phase for Ethane Oxidation. Microscopy and Microanalysis, 2016, 22, 790-791.	0.2	1
175	Imaging Electrochemical Processes in Li Batteries by Operando STEM. Microscopy and Microanalysis, 2017, 23, 1970-1971.	0.2	1
176	Controlling the Reaction Process in Operando STEM by Pixel Sub-Sampling. Microscopy and Microanalysis, 2017, 23, 98-99.	0.2	1
177	Manipulation and Immobilization of Nanostructures for In-situ STEM. Microscopy and Microanalysis, 2017, 23, 942-943.	0.2	1
178	Imaging and Analytical Approaches for Characterization of Soil Mineral Weathering. Microscopy and Microanalysis, 2017, 23, 2172-2173.	0.2	1
179	Mineral-Organic Interface on Clay Minerals: Imaging and Analytical Approaches. Microscopy and Microanalysis, 2019, 25, 2438-2439.	0.2	1
180	In-situ Observation of Ordering Transformations in Î,-Al ₂ O ₃ . Microscopy and Microanalysis, 2021, 27, 1956-1957.	0.2	1

#	Article	IF	CITATIONS
181	Understanding the microstructural stability in a γ′-strengthened Ni-Fe-Cr-Al-Ti alloy. Journal of Alloys and Compounds, 2021, 886, 161207.	2.8	1
182	Atom probe tomography and transmission electron microscopy: a powerful combination to characterize the speciation and distribution of Cu in organic matter. Environmental Sciences: Processes and Impacts, 0, , .	1.7	1
183	A Precession Electron Diffraction and EELS Study of Beta-phase Evolution in Nano-crystalline Mg-9 wt.% Al Thin Films during Heat Treatment. Microscopy and Microanalysis, 2015, 21, 1463-1464.	0.2	0
184	In Situ Environmental Transmission Electron Microscopy of Ice Nucleation. Microscopy and Microanalysis, 2015, 21, 425-426.	0.2	0
185	Correlative Imaging and Spectroscopy of Particles in Liquid. Microscopy and Microanalysis, 2016, 22, 220-221.	0.2	0
186	Direct Observation of Zirconium Alloy Oxidation at the Nanoscale. Microscopy and Microanalysis, 2019, 25, 318-319.	0.2	0
187	Multimodal Atomic Scale Characterization of Structural and Compositional Changes During Shear Deformation of Materials. Microscopy and Microanalysis, 2019, 25, 2510-2511.	0.2	0
188	Crystallographic Analysis of Transition Al2O3 Phases Under the Constrains of Complex Intergrowth and Disorder. Microscopy and Microanalysis, 2020, 26, 1532-1534.	0.2	0
189	Macro to Nanoscale Approaches to Study Mineral Transformations at the Liquid, Organic, Biological Interface Microscopy and Microanalysis, 2020, 26, 1568-1569.	0.2	0
190	Accelerated beta radiation aging of interlayer titanium nitride in gallium nitride contacts. MRS Communications, 2022, 12, 24.	0.8	0